

An Aerial Robot Prototype for Situational Awareness in Closed Quarters

William E. Green and Paul Y. Oh

Mechanical Engineering & Mechanics, Drexel University, Philadelphia PA

Email: weg22@drexel.edu and paul@coe.drexel.edu

Abstract

More often homeland security, disaster mitigation and military operations are performed in urban environments. Time consuming, labor intensive and possibly dangerous tasks like bomb detection, search-and-rescue and reconnaissance done with robots could save resources. An aerial robot capable of flying in closed quarters like warehouses, stadiums, underground parking lots and tunnels is featured. The working prototype can fly slowly, safely and transmit wireless video for situational awareness. The design is analytic and employs a multi-disciplinary design optimization to formulate the integration of aerodynamics, sensor suite and task performance.

1 Introduction

Milestones in aerial robots have been recently achieved using sensor suites that include GPS, inertial measurement units, laser altimeters, ultrasound and computer vision to perform missions like terrain-following, base station keeping and automated landing. Our particular interests in aerial robots however involve indoor environments that we call *closed quarters* – urban environments like stadiums, train stations, underground parking lots, subway tunnels and warehouses, which are spacious but enclosed (see Figure 1). Unfortunately much of the existing aerial robot literature revolving around sensor suite integration, path planning and navigation is not well suited for our flying environment; approaches working outdoors may not work in closed quarters. For example, GPS-based methods are of no use in closed quarters because satellite signals are occluded. Also, vision-based methods that reference the horizon (Pipitone et al [11]) are also inappropriate indoors.

Our interests stem from the observation that homeland security, disaster mitigation and military operations in closed quarters are time consuming, labor intensive and possibly dangerous. Tasks like search-and-rescue, bomb detection, and assessing a building's



Figure 1: Closed quarters like this multi-floor atrium are enclosed but spacious for aerial robots.

structural integrity are examples where many people are employed to canvass large areas in a short window of time. Our vision is to design a flying robot we call CQAR: *Closed Quarter Aerial Robot* (pronounced “seeker”) that can assist in such tasks. Examples include airlifting communication devices, cameras and biochemical sensors to eavesdrop, broadcast messages, observe hostages or casualties, assess structural damage or find explosives. We envision a CQAR fleet possibly supporting ground-based mobots (Blitch [3]) in such mission endeavors; an aerial robot could fly easily over stairs or ascend to the ceiling to capture larger fields-of-view, possibly assisting in mobot localization and motion planning.

In closed quarters, the aerial robot must fly safely and slowly to avoid damaging the area in case of collisions and small enough to fly through halls and possibly doorways. Building such a robot has become possible recently due to advances with Lithium-polymer batteries, lightweight materials like carbon fiber rods, small but powerful embedded micros, low-power sensors and high-torque miniature motors. Recently, Nicoud and Zufferey at EPFL in Lausanne Switzerland debuted an indoor aerial robot prototype [9].

Rotorcraft [14], [12], [8], blimps [15] and micro air vehicles, [6], may respectively be too dangerous, large or fast for closed quarters. However a hybrid vehicle like a blimp equipped with a ducted fan may be appropriate. The net effect is designing a closed quarter aerial robot cannot be done ad hoc. Rather, formulated design techniques like multidisciplinary design optimization become critical in understanding trade-offs in sensor selection, flight structure, aerodynamics and task performance.

This paper formulates a design prototype for a closed quarter aerial robot. First, the pros, cons and underlying dynamics contrasting lighter-than-air, rotary and fixed-wing vehicles are presented in Section 2. A matrix of design parameters along with our current prototype are presented in Sections 3 and 4 respectively. Section 5 concludes with autonomous landing metrics and near-future goals. As such the paper’s objective is to formulate and provide a set of guidelines in designing an aerial robot to fly in closed quarters, in and around buildings and possibly tunnels and caves.

2 Flight Modes

Lighter-than-air vehicles like blimps, rotorcraft like helicopters or ducted fan units [4], fixed and flapping-wing aircraft and tethered devices like kites [10] retrofitted with sensor suites are detailed in the aerial robotics literature. This section highlights and summarizes the underlying pros, cons and dynamics for various flight modes. Kites are not suited for closed quarters and are not discussed in this paper. Ornithopters [5], are currently being assessed and will be the subject of a future paper.

2.1 Lighter-than-air Vehicles

The most common gas used today in blimps is Helium, which has a lifting capacity of 0.064 lbs/ft^3 (1.02 kg/m^3). The helium makes the blimp positively buoyant in the surrounding air so that the blimp rises. Because gas provides the sufficient lifting force in blimps rather than wings and electric motors, blimps can remain airborne without expending fuel. This allows them to hover in the air for hours and days at a time, which is significantly longer than rotary and fixed-wing aircraft. The disadvantage for using blimps in closed quarters, however, is that a blimp’s buoyancy and inertial forces are proportional to its size. When flying in closed quarters for surveillance or search and rescue applications, it is essential to have a vehicle that can easily fit through a standard 3 foot doorway

or maneuver easily around pillars and hanging lights. Furthermore, because of its large inertial force, it is not able to quickly reverse directions.

The steering mechanisms of a blimp are typically stationed on the gondola which is attached to the Helium-filled blimp. The gondola sits below the center of gravity and hence most of the pitch and roll motion will be negligible. Zhang and Ostrowski [15] derived the blimp’s equations of motion to be

$$\begin{aligned} m_x a_x &= (T_1 + T_2) \cos \alpha - D_x \\ m_z a_z &= D_z + (T_1 + T_2) \sin \alpha \\ J_z \dot{\omega}_z &= (T_1 - T_2) l_y \cos \alpha + T_3 l_x + \tau_z \text{drag} \end{aligned}$$

2.2 Rotary-Wing Aircraft

Rotary-wing aircraft, like helicopters, are versatile, possessing the capability to hover, fly laterally and rotate 360 degrees. There are basically two types of r/c helicopters: those that have collective pitch and those that do not. Collective pitch is where the angle-of-attack of the main rotor blades may be simultaneously adjusted allowing the helicopter to increase or decrease its amount of lift. On helicopters with no collective pitch, the amount of lift is adjusted by changing the speed of the rotor. Most r/c helicopters today are collective pitch and are more expensive than fixed-wing aircraft. On a standard collective pitch helicopter, 5 channels of a radio system are required and are therefore much more complicated to control than airplanes or blimps.

The dynamics of rotary-wing aircraft are slightly more complex than lighter than air vehicles because they have twice the number of controls. Unlike lighter-than-air vehicles, which use helium, and fixed-wing aircraft, which rely on wings to generate lift, a helicopter’s main rotor supplies both the lift and thrust for the vehicle. This is achieved by tilting the rotor forward and the resolved forces move the aircraft horizontally while sustaining the required lift. The helicopter is assumed to be a rigid body in 3D space in order to streamline the dynamics. That is, when the rotor tilts, so does the fuselage. The free-body diagram of a helicopter in flight is shown in Figure 2 (left). θ , Ψ and ϕ are the rigid body rotations about the x -axis, y -axis and z -axis respectively. The thrust T , drag D and weight W forces are assumed to be acting about the center of gravity. τ_1 and τ_2 are the rotor reaction forces and ε is the angle between the free-stream velocity and the horizontal thrust vector. J is the moment of inertia about the helicopter’s center-

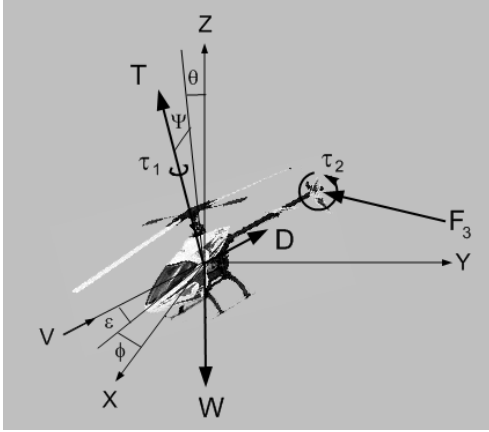


Figure 2: Free-body diagram of helicopter

of-gravity. Thus the equations of motion are

$$\begin{aligned}
 m_x a_x &= T \cos \theta \sin \Psi \cos \phi - D \cos \varepsilon \cos \theta \cos \Psi \cos \phi \\
 &\quad + F_{3_x} \\
 m_y a_y &= -T \sin \theta \cos \Psi \cos \phi + D \cos \varepsilon \cos \theta \cos \Psi \sin \phi \\
 &\quad + F_{3_y} \\
 m_z a_z &= T \cos \theta \cos \Psi \cos \phi + D \cos \varepsilon \cos \theta \sin \Psi \cos \phi \\
 &\quad + F_{3_z} - W
 \end{aligned}$$

$$\begin{aligned}
 J_x \dot{\omega}_x &= \tau_{1_x} + \tau_{2_x} + F_{3_z} l_y + F_{3_y} l_z \\
 J_y \dot{\omega}_y &= \tau_{1_y} + \tau_{2_y} + F_{3_z} l_x + F_{3_x} l_z \\
 J_z \dot{\omega}_z &= \tau_{1_z} + \tau_{2_z} + F_{3_x} l_y + F_{3_y} l_x
 \end{aligned}$$

2.3 Fixed-wing Aircraft

Literature describing the design of fixed-wing aircraft is vast with a long history. Such aircraft are both more cost efficient and stable than rotary-wing aircraft. During cruise flight, the governing design principle is that an aircraft's weight is proportional to its velocity

$$W = \frac{1}{2} \rho V^2 S C_L \quad (1)$$

From (1), a lighter aircraft means slower velocity requirements to maintain steady and level flight. This also corresponds to higher maneuverability, which is crucial for closed quarters. Until recently, the largest restriction for fixed-wing aircraft has been their inability to hover. However, slow speed aerodynamics permits large angles-of-attack without stall. For example, small, light aircraft can perform an aerobatic maneuver called prop hanging which mimics hovering. Here, the aircraft's angle-of-attack and thrust are simultaneously increased so that the fuselage is

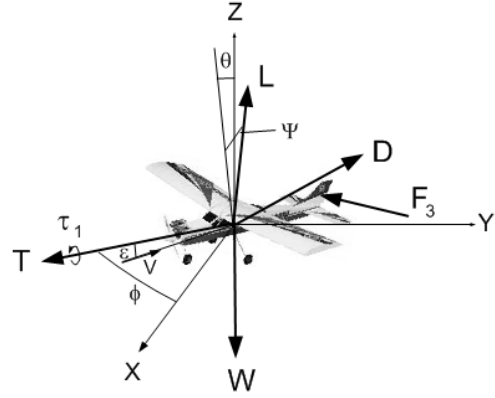


Figure 3: Free-body diagram of fixed-wing vehicle

vertical and the propeller is generating thrust in the downward direction.

The vehicle dynamics for fixed-wing aircraft are very similar to their rotary-wing counterparts when assumed to be rigid bodies [1]. The only differences are the propeller location and the absence of the tail rotor. However, the airplane's rudder and elevator compensate for this. The four forces of flight on a fixed-wing aircraft are lift L , drag D , thrust T and weight W and are sketched in Figure 3 (middle). θ , Ψ and ϕ are the rigid body rotations about the x , y and z axes respectively. τ_1 is the propeller's reaction force and the angle between the free-stream velocity and the thrust vector is ε . The four forces of flight and the moment of inertia J are about the airplane's center of gravity. Thus, the equations of motion for a fixed-wing aircraft in three-dimensional space are:

$$\begin{aligned}
 m_x a_x &= T \cos \theta \cos \Psi \cos \phi - D \cos \varepsilon \cos \theta \cos \Psi \cos \phi \\
 &\quad - L \cos \theta \sin \Psi \cos \phi + F_{3_x} \\
 m_y a_y &= -T \cos \theta \cos \Psi \sin \phi + D \cos \varepsilon \cos \theta \cos \Psi \sin \phi \\
 &\quad - L \sin \theta \cos \Psi \cos \phi + F_{3_y} \\
 m_z a_z &= T \cos \theta \sin \Psi \cos \phi - D \cos \varepsilon \cos \theta \sin \Psi \cos \phi \\
 &\quad - W + L \cos \theta \cos \Psi \cos \phi + F_{3_z}
 \end{aligned}$$

$$\begin{aligned}
 J_x \dot{\omega}_x &= \tau_{1_x} + F_{3_z} l_y + F_{3_y} l_z \\
 J_y \dot{\omega}_y &= \tau_{1_y} + F_{3_z} l_x + F_{3_x} l_z \\
 J_z \dot{\omega}_z &= \tau_{1_z} + F_{3_x} l_y + F_{3_y} l_x
 \end{aligned}$$

It can be seen from the equations above that $L = W$ and $T = D$ during cruise flight ($a_x = a_y = a_z = \theta = \Psi = \phi = 0$). Analyzing the dynamics of each platform helps formulate the metrics for an optimal design matrix.

3 Optimal Design Matrix

A closed quarter aerial robot demands understanding how aerodynamics, sensor suite integration and task description influence design. The metrics presented in the previous section can be parameterized into design variables. These variables can then be integrated to form a multi-disciplinary design optimization (MDO) matrix (Grasmeyer, Keennon [6]). The MDO method originated in the automobile industry [7] and has evolved into an invaluable discipline that supplies engineers with techniques to move engineering system design closer to optimal. Inputting some initial components into an MDO will yield the most applicable platform and its corresponding equations of motion.

Each design variable used has a large impact on platform selection (see Figure 5). The parameters that make up the design matrix include initial variables X_I , velocity variables X_V , size variables X_S , payload variables X_P , and hover variables X_H . The initial variables determine the mission type and include parameters such as environment (closed quarter, outdoors or both), desired tasks (search and rescue or reconnaissance), expendability, vertical takeoff and landing (VTOL) requirements, and stealthy operation. The velocity parameters are used to establish speed range capabilities. The size variables represent the platforms maximum characteristic length as well as propeller diameter. This will conclude whether or not the vehicle can fit through small openings like doorways. Payload variables determine the weight and dimensions of the designed sensor suite. The hover parameters assess whether or not there is a requirement and also the endurance of the hover. Common input parameters such as flight endurance, range or propeller geometry were not selected in this design matrix because such parameters can be manipulated once the optimal platform is selected. Based on the input parameters specified above, the program executes a series of commands to generate the most suitable aerial platform and its corresponding equations of motion. A graphical representation for the command sequence is shown in a flow chart (see Figure 4). The shaded boxes represent the input parameters of the user. Initially, a closed quarter environment and a search and rescue mission were specified which did not rule out any of the platforms. Next, the user wanted something that was expendable (roughly less than 300 USD) which eliminated more expensive rotorcraft as a possible solution for this mission. VTOL and stealthy operations were not required and

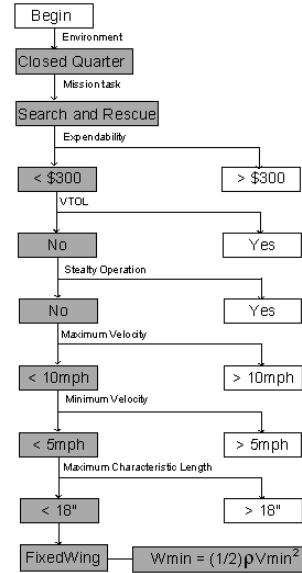


Figure 4: Flow chart detailing execution of commands

consequently, lighter than air vehicles and fixed-wing aircraft still remain. A velocity range (min to max) of 5 to 10 MPH was specified and likewise did not eradicate any of the remaining. However, because the maximum characteristic length was selected as less than 18-inches, lighter than air vehicles were eliminated (size is proportional to lift force) and fixed-wing aircraft was outputted as the optimal platform. All MAVs and most small fixed-wing vehicles can fly with a wing span less than 18-inches. Furthermore, the design matrix also yielded the platform dynamics which will allow the user to get an estimate of the aircraft's weight based on the inputs to the velocity matrix from (1). By selecting the most suitable aircraft and outputting its aerodynamic data, the MDO matrix will allow a more theoretical approach to the design and development of small autonomous aircraft prototypes.

4 CQAR Prototype

The fixed-wing flight mode and equations of motion ($L = W$ during cruise) generated by the design matrix allowed us to calculate the wing loading (W/S) for our aircraft (with a lift coefficient $C_L = 1$) using (1). Furthermore, using the desired cruise velocity of our aircraft (2 m/s), the room length can be calculated based on control system reaction time. That is, a plane traveling at 2 m/s would need a room length of 10 m in order for the control system to have 5 seconds to react. A graph was then created for several wing

X = Vector of input design variables

X	X_I	Initial variables
	X_V	Velocity variables
	X_S	Size variables
	X_P	Payload variables
	X_H	Hover variables
X_I	A_{OBJ}	Environment
	T_D	Desired Tasks
	C_{EXT}	Expendable
	$VTOL$	Vertical Takeoff and Landing Required
	O_{STEAM}	Stealthy Operation
X_V	V_{CRUISE}	Cruise Velocity ^c
	V_{MAX}	Maximum Velocity
	V_{MIN}	Minimum Velocity
X_S	b_{MAX}	Maximum Characteristic Length ⁺
	T_{PROP}	Propeller Diameter
X_P	W_P	Payload Weight
	l_P	Payload Length
	w_P	Payload Width
	h_P	Payload Height
X_H	R_{HOVER}	Hover Requirement
	L_{HOVER}	Maximum Hover Length

* If indoors, will it need to withstand wind gusts
+ 3 foot (or less) to fit through standard doorways
c Used for calculations only - not platform selection

Figure 5: Design matrix input parameters

loading scenarios (see Figure 6). From the graph, it can be seen that a weight of less than 30 g was required to fly in a room that is 10 m long. A prototype based on the output from the design optimization matrix and the graph was constructed out of carbon fiber rods, lightweight balsa wood and 3 μ m mylar covering. The resulting vehicle can carry a 14 g sensor payload and navigate in a 10 \times 10 m^2 area (about 1/3 the size of a basketball court) when flying at a maximum speed of 2 m/s (about the speed of a slow jogging person).

With this payload capacity, the aircraft can carry a lightweight mini wireless camera and power supply as shown in Figure 7 (left). The middle photo is a frame captured by the on-board camera while flying in the atrium (Figure 1). A table can be identified, but the image is noisy. We are currently testing more robust wireless cameras to eliminate the imperfections due to the wireless camera's poor performance.

5 Conclusions and Future Work

Closed quarters which are enclosed but spacious areas like warehouses, stadiums, underground parking lots and tunnels, are time consuming and labor intensive to patrol and safe keep. A robot designed to fly in closed quarters and deliver situational awareness would benefit homeland security, disaster mit-

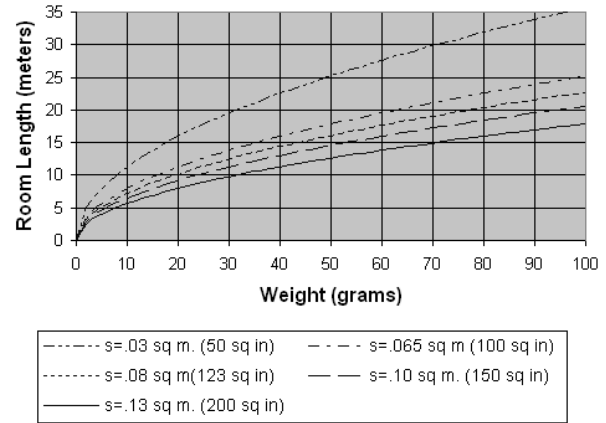


Figure 6: Room size versus weight graph for different fixed-wing areas

igation and military operations. Applications could include biochemical detection, search-and-rescue and reconnaissance. This paper presented a working prototype based on output from a optimization matrix that parameterized design variables. Parameterization considered the pros and cons of different flight modes, namely lighter-than-air and both rotary and fixed-wing aircraft. The resulting closed quarter aerial robot (CQAR) can fly safely and slowly in an area as small as 10 \times 10 square meters and deliver wireless video with its on-board camera.

An optic flow sensor suite that can achieve autonomous landing for perch-and-stare surveillance is currently being designed (see Figure 7 (right)). The use of optic flow for navigation was inspired by insects which make heavy use of vision, especially optic flow, for perceiving the environment. When approaching an autonomous takeoff or landing (ATOL), the optic flow in the downward direction is equivalent to the vehicle's forward velocity, v , over the current altitude, d . Our ATOL control system follows Srinivasan's observation that insects keep the optic flow on the landing surface constant when approaching a landing, [13]. Thus, an embedded microprocessor is used to gradually decrease the motor speed over a period of 20 seconds while simultaneously controlling the vehicle's pitch (elevator) to maintain a constant optic flow reading from the Ladybug optic flow sensor, [2], (i.e. a large jump in the optic flow calls for a large deflection of the elevator). We are currently collecting data from initial test results and comparing them to the formulated ATOL metrics which include: force of ground impact, or lack of bounce, overshoot or un-

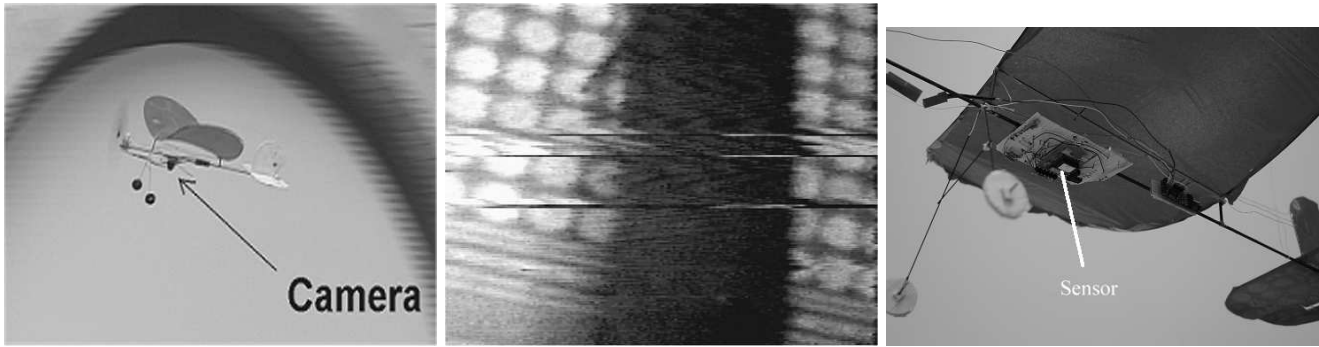


Figure 7: An on-board wireless camera mounted on the flying prototype (left) can acquire video and transmit images. The raw image in the middle is of a banquet table. An optic flow sensor suite (right) is used to achieve autonomous takeoffs and landings.

dershoot from a landing target, distance from runway centerline, and maintaining stability throughout the landing sequence (keeping pose constant).

Acknowledgements: We thank Jean-Christophe Zufferey of the Swiss Federal Institute of Technology (EPFL) in Lausanne Switzerland for his advice and suggestions in our CQAR prototype. We also thank microflight aircraft designer Gordon Johnson and David Lewis of Homefly Inc., for their hardware and construction suggestions.

References

- [1] Anderson, J.D., *Aircraft Performance and Design*, McGraw-Hill, 1999.
- [2] Barrows, G., Neely, C., “Mixed-mode VLSI Optic Flow Sensors for In-flight Control of a Micro Air Vehicle”, *Proc. SPIE*, 4109 pp. 52-63, 2000.
- [3] Blitch, J., “World Trade Center Search-and-Rescue Robots”, Plenary Session *IEEE Int Conf Robotics and Automation*, Washington D.C., May 2002.
- [4] Choi, H., Sturdza, P., Murray, R.M., “Design and Construction of a Small Ducted Fan Engine for Non-linear Control Experiments”, *Proc. American Control Conf.*, Baltimore MD, pp. 2618-2622, June 1994.
- [5] Fearing, R., et al, “Wing Transmission for a Micromechanical Flying Insect”, *IEEE Int Conf Robotics and Automation*, San Francisco pp. 1509-1516, April 2000.
- [6] Grasmeyer, J.M., Keennon, M.T., “Development of the Black Widow Micro Air Vehicle”, *39th AIAA Aerospace Sciences Meeting and Exhibit*, Reno, NV, Jan. 2001.
- [7] Kodiyalam, S., Sobieszczanski-Sobieski, J., “Multidisciplinary Design Optimization - Some Formal Methods, Framework Requirements, and Application to Vehicle Design”, *Int. Journal of Vehicle Design (Special Issue)*, pp. 3-22.
- [8] Hamel, T.; Mahony, R., Chriette, A., “Visual Servo Trajectory Tracking for a Four Rotor VTOL Aerial Vehicle”, *IEEE International Conference on Robotics and Automation (ICRA)*, Washington, D.C., pp. 2781-2786, 2002.
- [9] Nicoud, J.D., Zufferey, J.C., “Toward Indoor Flying Robots”, *IEEE/RSJ Int Conf on Robots and Systems*, Lausanne, pp. 787-792, October 2002.
- [10] Oh, P.Y., Green, W.E., “A Kite and Teleoperated Vision System for Acquiring Aerial Images”, *IEEE International Conference on Robotics and Automation (ICRA)*, Taipei, Taiwan 2003 (in press).
- [11] Pipitone, F., Kamgar-Parsi, B., Hartley, R., “Three Dimensional Computer Vision for Micro Air Vehicles”, *Proc. SPIE 15th Aerosense Symposium*, Conf. 4363, Enhanced and Synthetic Vision 2001, Orlando Florida, April 2001.
- [12] Sharp, C.S., Shakernia, O., Sastry, S.S., “A Vision System For Landing an Unmanned Aerial Vehicle *IEEE International Conference on Robotics and Automation (ICRA)*, Seoul, Korea, pp. 1720-1727, 2001.
- [13] Srinivasan, M.V., Chahl, J.S., Weber, K., Venkatesh, S., Nagle, M.G., Zhang, S.W., *Robot Navigation Inspired By Principles of Insect Vision* in Field and Service Robotics, A. Zelinsky (ed), Springer Verlag Berlin, NY 12-16.
- [14] Saripalli, S., Montgomery, J.F., Sukhatme, G.S., “Vision-based Autonomous Landing of an Unmanned Aerial Vehicle”, *IEEE International Conference on Robotics and Automation (ICRA)*, Washington, D.C., pp. 2799-2804, 2002.
- [15] Zhang, H., Ostrowski, J.P., “Visual Servoing With Dynamics: Control of an Unmanned Blimp”, *IEEE International Conference on Robotics and Automation (ICRA)*, Detroit, pp. 618-623, 1999.